BEM Solution in the Time Domain for a Moving Time-Dependent Force

Rasmussen, K. M.; Nielsen, Søren R. K.; Kirkegaard, Poul Henning

Publication date:
1999

Document Version
Accepted author manuscript, peer reviewed version

BEM Solution in the Time Domain for a Moving Time-Dependent Force Force

K.M. Rasmussen, S.R.K. Nielsen & P.H. Kirkegaard

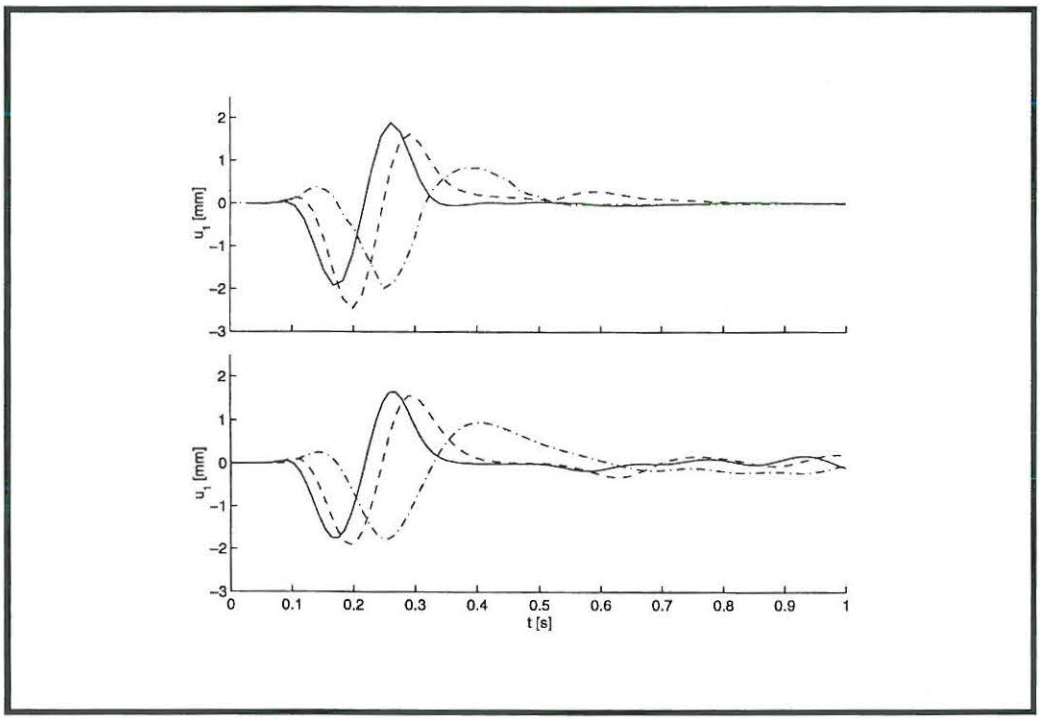

Submitted to Computers and Structures

Structural Dynamics, Paper No. 10
Aalborg University
juli 1999

ISSN 1395 7953 R9902
Dept. of Building Technology and Structural Engineering
Aalborg University
Sohngaardsholmsvej 57, DK-9000 Aalborg
Phone: +45 9635 8080 Fax: +45 9814 8243

BEM solution in the time domain for a moving time-dependent force

K.M. Rasmussen, S.R.K. Nielsen & P.H. Kirkegaard

Department of Building Technology and Structural Engineering
Aalborg University, Sohngaardsholmsvej 57, DK-9000 Aalborg, Denmark
Tel.:+45 96358583 Fax:+45 98148243
email: i6kmr@civil.auc.dk

Abstract

The problem of a moving time dependent concentrated force on the surface of an elastic halfspace is of interest in the analysis of traffic generated noise. The BEM is superior to the FEM in solving such problems due to its inherent ability so satisfy the radiation conditions exactly. In this paper a model based on the BEM is formulated for the solution of the mentioned problem. A numerical solution is obtained for the 2D plane strain case, and comparison is made with the results obtained from a corresponding FEM solution with an impedance absorbing boundary condition.

Key words: Boundary element method, moving force, wave propagation, stress waves, soil dynamics.

1 Introduction

Traffic induced vibrations are known sources of discomfort and damage problems in nearby buildings, either directly in the form of vibrations of the buildings or through structure borne acoustic noise, Okumura et al. [9], Trochides [12]. During the last couple of decades highway induced noise has become an increasing problem due to the increase of the general amount of traffic. Besides the average weight and velocity of trucks have increased significantly, which further has emphasized the problems of traffic induced vibrations. Also train induced vibrations have been given some attention in recent years, mainly due to the dramatic increase in speed, Krylov [6]. The increased speed and the still greater number of underground railway systems in urban areas have resulted in still larger vibration problems. An considerable effort has been made to minimize or soften the effects of the trafic induced vibrations, Chouw et al. [2], Nelson [8]. With respect to analysis, semi-empirical methods for estimating

the vibrations have been introduced, Madshus et al. [7], and some numerical methods used to estimate the vibrations have been introduced, but mainly in the frequency domain.
Simulation of traffic induced vibrations in an elastic medium can be achieved as a sum of moving concentrated time-varying forces due to the superposition principle. Thus, the basic problem that must be solved to simulate traffic induced vibrations is the problem of a moving time dependent force on the surface of an elastic halfspace. When using the BEM or FEM to solve this problem an important problem arises. With an element mesh of finite size the moving force will soon move beyond the boundary of the mesh. Therefore, it will be preferable to formulate the problem in a coordinate system moving along with the force, i.e. a convective formulation should be used.
FEM formulations in convected coordinates where the mesh is following the force are well known. If this is coupled with transmitting boundaries an efficient method for modelling transient problems of moving forces on infinite media arises, see e.g. Krenk et al. [5].
In this paper Green's functions in the time domain for the displacements and surface tractions are formulated in a coordinate system moving along with the force. Thereby a BEM formulation in a moving coordinate system is established similar to the method of coupling convected coordinates with absorbing boundaries for the FEM. Numerical results obtained by the BEM have been indicated for a 2D plane strain problem, and the results are compared to those obtained by the FEM.

2 Formulation of boundary element equations for a moving force

Let $U_{ik}(\mathbf{x}, t; \boldsymbol{\xi})$ signify the displacement field in the coordinate direction i from a concentrated time dependent force $f(t)$ applied at position $\boldsymbol{\xi}$ in direction k in a homogeneous, isotropic and linear elastic medium with the Lamé constants λ and μ and the mass density ρ. Assuming the media at rest at the time $t = 0$ the displacement is given as

$$U_{ik}(\mathbf{x}, t; \boldsymbol{\xi}) = \int_0^t g_{ik}(\mathbf{x}, t; \boldsymbol{\xi}, \tau) f(\tau) \mathrm{d}\tau \tag{1}$$

Green's function for the displacement field $g_{ik}(\mathbf{x}, t; \boldsymbol{\xi}, \tau)$ is the solution to the differential equations

$$\frac{\partial \sigma_{ijk}}{\partial x_j} - \rho \frac{\partial^2 g_{ik}}{\partial t^2} + \delta_{ik} \delta(\mathbf{x} - \boldsymbol{\xi}) \delta(t - \tau) = 0 \tag{2}$$

$\sigma_{ijk}(\mathbf{x}, t; \boldsymbol{\xi}, \tau)$ is the stress tensor derived from the displacement field $g_{ik}(\mathbf{x}, t; \boldsymbol{\xi}, \tau)$, δ_{ik} is the Kronecker's delta and $\delta(t)$ is the Dirac's delta function. Further, the summation convention for Cartesian tensors has been used. Next, consider a concentrated force moving at a constant velocity v_i in a linear elastic media, see Fig. 1.

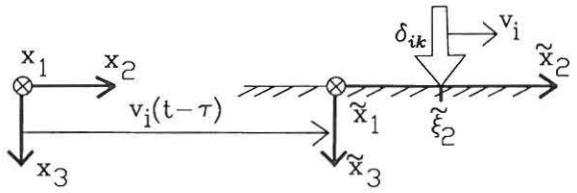

Fig. 1. Moving force in fixed and moving coordinate systems.

Next, a $(\tilde{x}_1, \tilde{x}_2, \tilde{x}_3)$-coordinate system is introduced, which follows the moving force. $\tilde{\xi}_i$ signifies the coordinates of the force, and $\tilde{g}_{ik}(\tilde{\mathbf{x}}, t; \tilde{\boldsymbol{\xi}}, \tau)$ is the Green's function for the displacement $\tilde{u}_i(\tilde{\mathbf{x}}, t)$ in the moving coordinate system. The two coordinate systems coalesce at the time $t = \tau$ which corresponds to the Galilean transformation

$$x_i = \tilde{x}_i + v_i(t - \tau) \tag{3}$$

The equations of motion in the moving coordinate system are expressed by introducing the partial differentiation operators

$$\left.\begin{aligned} \frac{\partial}{\partial x_j} &= \frac{\partial}{\partial \tilde{x}_j} \\ \left.\frac{\partial}{\partial t}\right|_{x_j} &= \left.\frac{\partial}{\partial t}\right|_{\tilde{x}_j} - v_j \frac{\partial}{\partial \tilde{x}_j} \\ \left.\frac{\partial^2}{\partial t^2}\right|_{x_j} &= \left.\frac{\partial^2}{\partial t^2}\right|_{\tilde{x}_j} - 2v_j \left.\frac{\partial^2}{\partial \tilde{x}_j \partial t}\right|_{\tilde{x}_j} + v_j v_k \frac{\partial^2}{\partial \tilde{x}_j \partial \tilde{x}_k} \end{aligned}\right\} \tag{4}$$

Hereby the partial differential equations for the Green's functions in the moving coordinate system read

$$\begin{aligned} &\frac{\partial \tilde{\sigma}_{ijk}}{\partial \tilde{x}_j} - \rho \left(\frac{\partial^2 \tilde{g}_{ik}}{\partial t^2} - 2v_j \frac{\partial^2 \tilde{g}_{ik}}{\partial \tilde{x}_j \partial t} + v_j v_l \frac{\partial^2 \tilde{g}_{ik}}{\partial \tilde{x}_j \partial \tilde{x}_l} \right) \\ &+ \delta_{ik} \delta(\tilde{\mathbf{x}} - \tilde{\boldsymbol{\xi}}) \delta(t - \tau) = 0 \end{aligned} \tag{5}$$

Introducing the coordinate transformation (3) into (5) the following equations for $\tilde{g}_{ij}$ is found as a function of the fixed coordinates x_i

$$\frac{\partial \tilde{\sigma}_{ijk}}{\partial x_j} - \rho \frac{\partial^2 \tilde{g}_{ik}}{\partial t^2} + \delta_{ik} \delta(\mathbf{x} - \mathbf{v}(t - \tau) - \tilde{\boldsymbol{\xi}}) \delta(t - \tau) = 0 \tag{6}$$

Since $\delta(\mathbf{x}-\mathbf{v}(t-\tau)-\tilde{\boldsymbol{\xi}})\delta(t-\tau) = \delta(\mathbf{x}-\tilde{\boldsymbol{\xi}})\delta(t-\tau)$, the solution of (6) becomes $g_{ik}(\mathbf{x},t;\tilde{\boldsymbol{\xi}},\tau)$. The solution to (5) can then be expressed in terms of the Green's function for the displacement field in the fixed coordinate system in the following way

$$\tilde{g}_{ik}(\tilde{\mathbf{x}},t;\tilde{\boldsymbol{\xi}},\tau) = g_{ik}(\mathbf{x},t-\tau;\tilde{\boldsymbol{\xi}},0) = g_{ik}(\tilde{\mathbf{x}}+\mathbf{v}(t-\tau),t-\tau;\tilde{\boldsymbol{\xi}},0) \tag{7}$$

The Green's function for Cauchy's stress tensor $\tilde{\sigma}_{ijk}(\tilde{\mathbf{x}},t;\tilde{\boldsymbol{\xi}},\tau)$ is obtained upon insertion of the solution of (7) into the constitutive equations for the considered linear elastic material. Since these only involve spatial differential operations with respect to $\mathbf{x}$, the result is seen to be

$$\tilde{\sigma}_{ijk}(\tilde{\mathbf{x}},t;\tilde{\boldsymbol{\xi}},\tau) = \sigma_{ijk}(\tilde{\mathbf{x}}+\mathbf{v}(t-\tau),t-\tau;\tilde{\boldsymbol{\xi}},0) \tag{8}$$

Hence, a BEM formulation in the moving coordinate system that calculates the displacement field following the force can be established by using the formal Green's functions $\tilde{g}_{ik}(\tilde{\mathbf{x}},t;\tilde{\boldsymbol{\xi}},\tau)$ and $\tilde{\sigma}_{ijk}(\tilde{\mathbf{x}},t;\tilde{\boldsymbol{\xi}},\tau)$, as given by (7) and (8), instead of the original ones. Notice that this result is generally valid for linear materials whether these are homogeneous and isotropic or not.

3 Boundary element formulation

Green's function for the displacement field in linear elastic homogeneous and isotropic fields, $g_{ij}(\mathbf{x},t;\boldsymbol{\xi},0)$ is well known and can be found in e.g. Eringen and Suhubi [3].

$$g_{ik}(\mathbf{x},t;\boldsymbol{\xi},0) = \frac{1}{4\pi\rho}\Bigg\{\left(\frac{3r_ir_k}{r^3}-\frac{\delta_{ik}}{r}\right)\int_{c_P^{-1}}^{c_S^{-1}}\kappa\delta(t-\kappa r)\mathrm{d}\kappa + \\ \frac{r_ir_k}{r^3}\left(\frac{1}{c_P^2}\delta\left(t-\frac{r}{c_P}\right)-\frac{1}{c_S^2}\delta\left(t-\frac{r}{c_S}\right)\right)+\frac{\delta_{ik}}{rc_S^2}\delta\left(t-\frac{r}{c_S}\right)\Bigg\} \tag{9}$$

where $r = |\mathbf{x}-\boldsymbol{\xi}|$, $r_i = x_i-\xi_i$ and $c_P = \sqrt{\frac{\lambda+2\mu}{\rho}}$ and $c_S = \sqrt{\frac{\mu}{\rho}}$ denotes the phase velocities of P- and S-waves.
Green's function for the surface traction in 3D, $t_{ik}(\mathbf{x},t;\boldsymbol{\xi},0)= \sigma_{ijk}(\mathbf{x},t;\boldsymbol{\xi},0)n_j(\mathbf{x})$, where $n_j(\mathbf{x})$ is the outward directed unit vector, can be derived from $g_{ik}(\mathbf{x},t;\boldsymbol{\xi},0)$ in a straight forward manner.
Using the Betti reciprocal theorem and the symmetry properties of Green's functions, Somigliana's identity in 3D is obtained.

$$C(\mathbf{x})u_i(\mathbf{x},t) = \int_S \int_0^t g_{ik}(\mathbf{x},t-\tau;\boldsymbol{\xi},0)t_k(\boldsymbol{\xi},\tau;\mathbf{n}(\boldsymbol{\xi}))\mathrm{d}\tau\mathrm{d}S_{(\boldsymbol{\xi})} -$$

$$\oint_S \int_0^t \sigma_{ijk}(\mathbf{x},t-\tau;\boldsymbol{\xi},0)n_j(\mathbf{x})u_k(\boldsymbol{\xi},\tau)\mathrm{d}\tau\mathrm{d}S_{(\boldsymbol{\xi})} \tag{10}$$

$C(\mathbf{x})$ is a parameter which is 1 for $\mathbf{x}$ in the interior, 0 for $\mathbf{x}$ in the exterior and $1/2$ for $\mathbf{x}$ on the surface of the domain if the surface is smooth. For surface points with sharp corners special attention is needed. Discretization of Somigliana's identity in 3D yields

$$C(\mathbf{x})u_i^+(\mathbf{x},t) =$$
$$\sum_{m=1}^{M}\sum_{n=1}^{N}\int_{S^m} g_{ik}(\mathbf{x},t;\boldsymbol{\xi}(\boldsymbol{\eta}),0) * N^{(m,n)}(\boldsymbol{\eta})\cdot t_k^{(m,n)}(t)\det(\mathbf{J}^{(m)}(\boldsymbol{\eta}))\mathrm{d}S_{(\boldsymbol{\eta})}$$
$$-\sum_{m=1}^{M}\sum_{n=1}^{N}\int_{S^m} t_{ik}(\mathbf{x},t;\boldsymbol{\xi}(\boldsymbol{\eta}),0) * N^{(m,n)}(\boldsymbol{\eta})u_k^{(m,n)}(t)\det(\mathbf{J}^{(m)}(\boldsymbol{\eta}))\mathrm{d}S_{(\boldsymbol{\eta})} \tag{11}$$

where M is the number of elements into which the surface has been divided, N is the number of nodal points within each element, $*$ is an operator indicating the convolution integral over time, η is the local axis over which the integration is performed, $N^{(m,n)}(\boldsymbol{\eta}a)$, $\det(\mathbf{J}^{(m)}(\boldsymbol{\eta}))$, $t_k^{(m,n)}(t)$ and $u_k^{(m,n)}(t)$ are the shape functions, the Jacobian and the nodal values of the displacement field belonging to element m. The integration in (11) over the surface S_m is performed numerically in the $\boldsymbol{\eta}$-coordinates defining the element which are mapped into $\boldsymbol{\xi} = \boldsymbol{\xi}(\boldsymbol{\eta})$ coordinates by an isoparametric mapping. The disturbance from a given impulse at a source point is limited by the wave front of the P- and S-waves. Before and after these wave fronts the medium is at rest. In order to improve the accuracy and stability the numerical surface integral in (11) should concentrate on such parts of the element which are emcompassed by the wave fronts. Such a wave front based integration was originally developed by Rasmussen and Nielsen [11] for the case of a stationary force, where the wave propagation appears as concentric circles on a plane surface. In the present case of a moving force the method has been modified to take into consideration the ellipsoidal nonhomogeneous wave propagation defined by the distance $\tilde{r}(t) = \sqrt{(\tilde{x}_1 + v_1 t - \tilde{\xi}_1)^2 + (\tilde{x}_2 + v_2 t - \tilde{\xi}_2)^2}$. Since the discontinuities of the wave front are well defined it is easy to discretize the wave front into elements. The integration is further enhanced by using directional subdivision. Evaluation of the singular integrals for the Green functions for $\mathbf{x} = \boldsymbol{\xi}$ is made using enclosing elements and the wellknown rigid-body motion principle, see e.g. Banerjee et al. [1].
The BEM equations have been formulated for both the direct and indirect

versions of the BEM in the time domain, see Rasmussen and Nielsen [11].

4 Time approximation

For the time integration in (11) the time interval $[0, t]$ is divided into L subintervals, each of the length $\Delta t = \frac{t}{L}$. A linear variation of the field variables during each time step is assumed. Hereby two shape functions for the time integration are necessary and the following two integrals need to be evaluated analytically, Rasmussen [10]

$$G_{ik}^{(1)} = \int_{t_{l-1}}^{t_1} g_{ik}(\tilde{\mathbf{x}} + \mathbf{v}(t-\tau), t-\tau; \tilde{\boldsymbol{\xi}}, 0)(1-\kappa_l)\mathrm{d}\tau \tag{12}$$

$$G_{ik}^{(2)} = \int_{t_{l-1}}^{t_1} g_{ik}(\tilde{\mathbf{x}} + \mathbf{v}(t-\tau), t-\tau; \tilde{\boldsymbol{\xi}}, 0)\kappa_l\mathrm{d}\tau \tag{13}$$

where the space integration has been omitted and $\kappa_l = \frac{\tau - t_{l-1}}{\Delta t}$. Similar integrals appear for Green's function for the surface traction for a moving force.
Analytical integration of (12) and (13), as well as the corresponding results involving the Green function for the surface traction is necessary since the later spatial integration into (11) will otherwise become unnecessarily complex, time consuming and inaccurate. The analytical integration of the discontinuous functions is made by splitting the integration up into several parts depending on the relationship between time variation of the discontinuous functions and the integration limits, see Rasmussen [10].

5 FEM solution with absorbing boundaries

A FEM formulation in convected coordinates is obtained by discretization of field differential equations similar to (6) for the displacement $\tilde{u}_i(\tilde{\mathbf{x}}_j, t)$. At the artificial boundary of the mesh absorbing boundary conditions for the surface tension t_i need to be specified as

$$t_i = -Z_{ij}\left(\dot{\tilde{u}}_j - v_k\frac{\partial \tilde{u}_j}{\partial \tilde{x}_k}\right) \tag{14}$$

A general impedance tensor Z_{ij} for absorption of plane P- and S-waves in a fixed coordinate system was derived by Krenk and Kirkegaard [4]. The correction (14) for moving coordinates is due to Krenk et al. [5]. The proposed impedance tensor Z_{ij} takes into account that the directions of propagation of plane P- and S-waves when observed in a point in the moving coordinate system are not identical, even when originally from the same source.
The final FEM equations are not symmetric due to the asymmetries from the convection terms in the field equations and due to the absorbing boundary conditions. This tend to destabilise the numerical results at large Mach-numbers ($M = \frac{v_1}{c_S}$) and has been cured using a technique similar to the partial upwinding in Petrov-Galerkin variation, see Krenk et al. [5].
Since the impedance boundary condition has been tuned to plane P- and S-waves. Therefore, Rayleigh, Love, Stoneley and non-plane P- and S-waves are partially reflected. The impedance boundary condition of the type (14) is not able to sustain static loading. Further, permanent displacements occur if the net impulse $\int_{-\infty}^{\infty} \mathbf{P}(t)\mathrm{d}t \neq \mathbf{0}$, where $\mathbf{P}(t)$ is nodal loadings.

6 Numerical example

The problem of a time-dependent load with zero net-impulse on an isotropic, homogenous linear elastic 2D plane strain halfspace is analysed using both the BEM and FEM approaches. The medium is subjected to a moving time dependent surface load per unit length $P(t)$. The time variation of the load is given as

$$\left.\begin{aligned} P(t) &= P_0\tau(1-\tau^2)^2 \\ \tau &= 2t/T - 1 \quad , \quad -1 < \tau < 1 \end{aligned}\right\} \tag{15}$$

P_0 is the amplitude of the load, which appears almost sinusonidally with the period T. However, the load has vanishing derivatives at $t = 0$ and $t = T$.
The example is performed with the following parameters : Intensity of force $P_0 = 1$ MN, $\mu = \lambda = 100 \cdot 10^6$ N/m^2 and $\rho = 2.0 \cdot 10^3$ kg/m^3. This gives the wave velocities for the P-, S- and Rayleigh waves, respectively, $c_P = 387$ m/s, $c_S = 224$ m/s and $c_R = 206$ m/s.
160 m of the surface are discretized and the force is applied at the centre. The applied FEM mesh is rectangular with a depth of 80 m. The BEM mesh consists of 4 m, 2 node, line elements with linear interpolation and similarly the FEM mesh consists of 4 m by 4 m, 4 node quadrilateral elements, see Fig. 2 a, b.

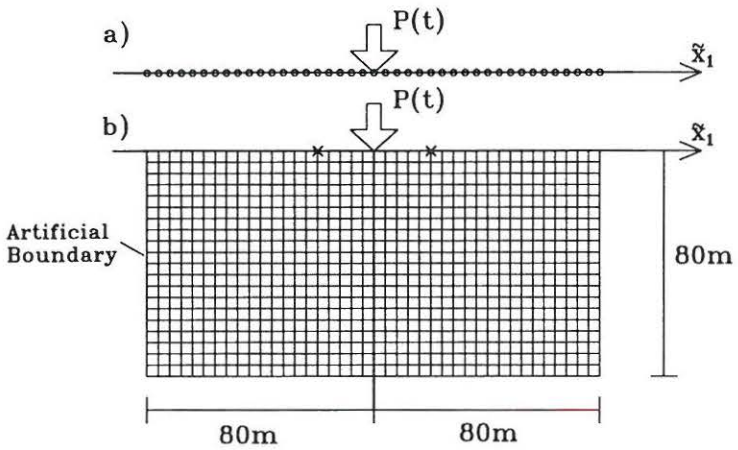

Fig. 2. a) BEM and b) FEM meshes.

The horizontal, u_1 and vertical, u_2 displacement histories at $(\tilde{x}_1, \tilde{x}_2, \tilde{x}_3) =$ (+20 m, 0 m, 0 m), 'in front of the force' and at $(\tilde{x}_1, \tilde{x}_2, \tilde{x}_3) =$ (-20 m, 0 m, 0 m), 'behind the force' are presented in the following figures.

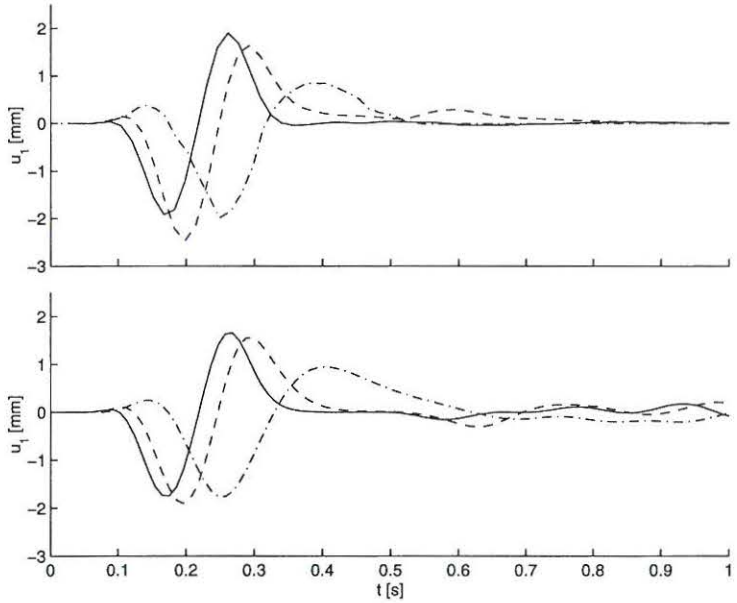

Fig. 3. Horizontal displacements at $(\tilde{x}_1, \tilde{x}_2, \tilde{x}_3)$=(+20 m, 0 m, 0 m) obtained using BEM (top) and FEM (bottom) for $v_1 = 0 \cdot c_S$ $-$, $v_1 = 0.2 \cdot c_S$ $--$ and $v_1 = 0.5 \cdot c_S$ $-\cdot-$.

The applied counter measure to stabilize the FEM scheme due to the convection terms is tantamount to the introduction of artificial numerical damping, which may change the magnitude of the observed response slightly. This defect should be kept in mind in the following comparison with the BEM solution. Comparison between Fig. 3 and Fig. 4 shows that both the minimum and maximum displacements decrease with greater speed. However, for $v_1 = 0 \cdot c_S$ in Fig. 3, the BEM results for the minimum displacements are significantly smaller than the equivalent minima from the FEM results. The solution of the time integrals of the Green functions becomes unstable when v_1 approaches

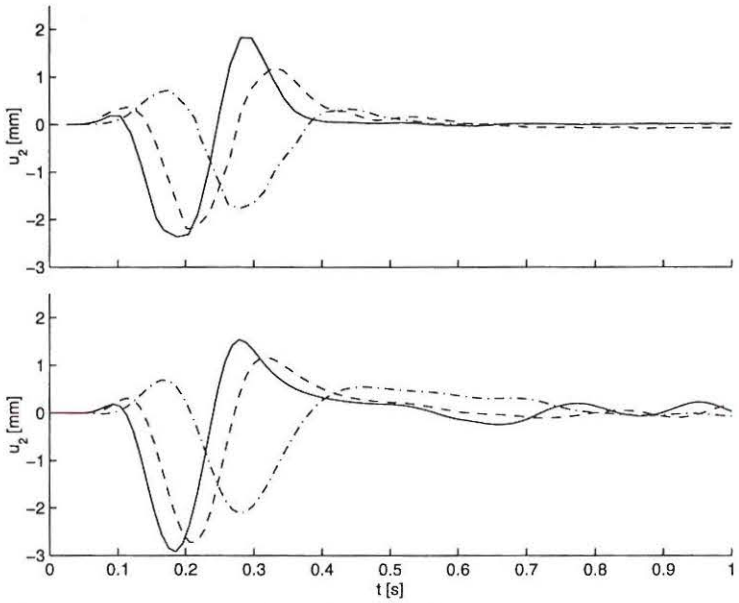

Fig. 4. Vertical displacements at $(\tilde{x}_1, \tilde{x}_2, \tilde{x}_3)$=(+20 m, 0 m, 0 m) obtained using BEM (top) and FEM (bottom) for $v_1 = 0 \cdot c_S$ $-$, $v_1 = 0.2 \cdot c_S$ $--$ and $v_1 = 0.5 \cdot c_S$ $- \cdot -$.

zero. Therefore, the results for very small velocities obtained by the BEM are not reliable.

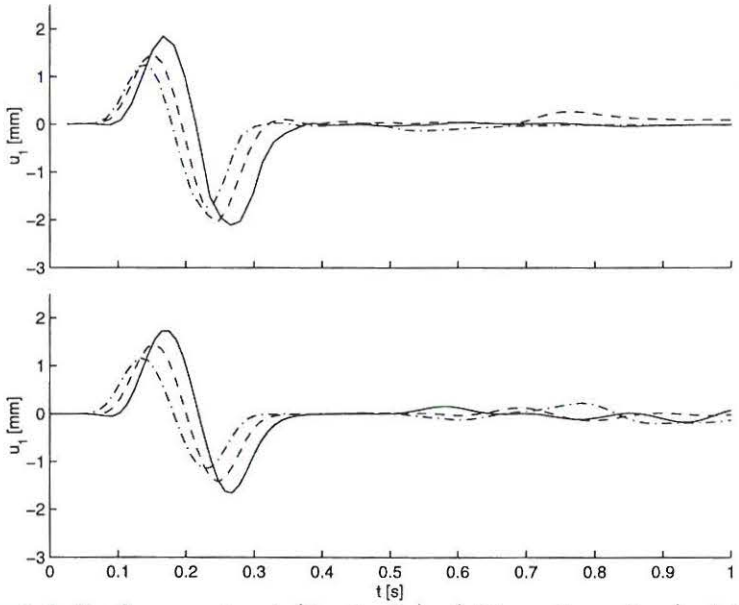

Fig. 5. Horizontal displacements at $(\tilde{x}_1, \tilde{x}_2, \tilde{x}_3)$=(-20 m, 0 m, 0 m) obtained using BEM (top) and FEM (bottom) for $v_1 = 0 \cdot c_S$ $-$, $v_1 = 0.2 \cdot c_S$ $--$ and $v_1 = 0.5 \cdot c_S$ $- \cdot -$.

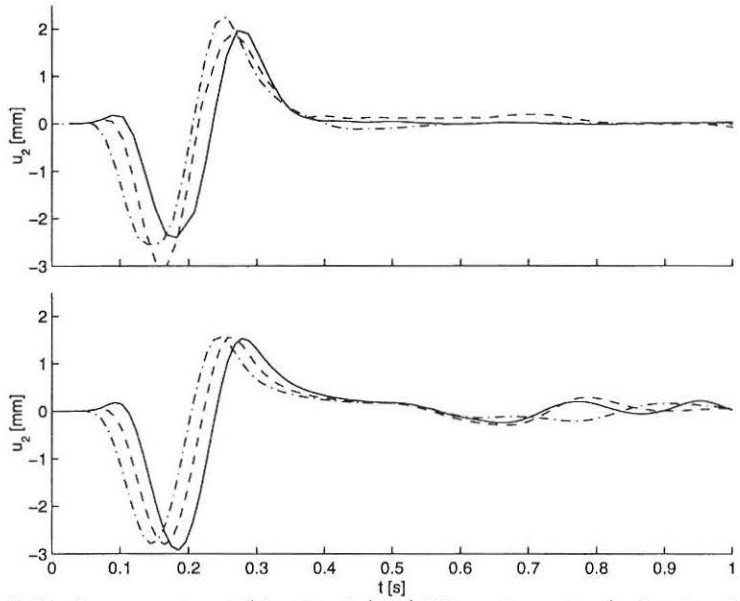

Fig. 6. Vertical displacements at $(\tilde{x}_1, \tilde{x}_2, \tilde{x}_3)$=(-20 m, 0 m, 0 m) obtained using BEM (top) and FEM (bottom) for $v_1 = 0 \cdot c_S$ $-$, $v_1 = 0.2 \cdot c_S$ $--$ and $v_1 = 0.5 \cdot c_S$ $-\cdot-$.

In all the Fig. 3-6, but especially in Fig. 6, the FEM results show tendencies to reflect Rayleigh waves from the boundaries. However, the BEM results do not show any signs of reflection in any of the figures. The calculation time for the FEM solution was 62 seconds on a 200 MHz PC while the calculation time for the BEM solution was several hours on a SiliconGraphics Indy R4400.
In Fig. 7-8 the FEM and BEM results for velocities approaching the Rayleigh wave velocity are shown 'in front of the force'.

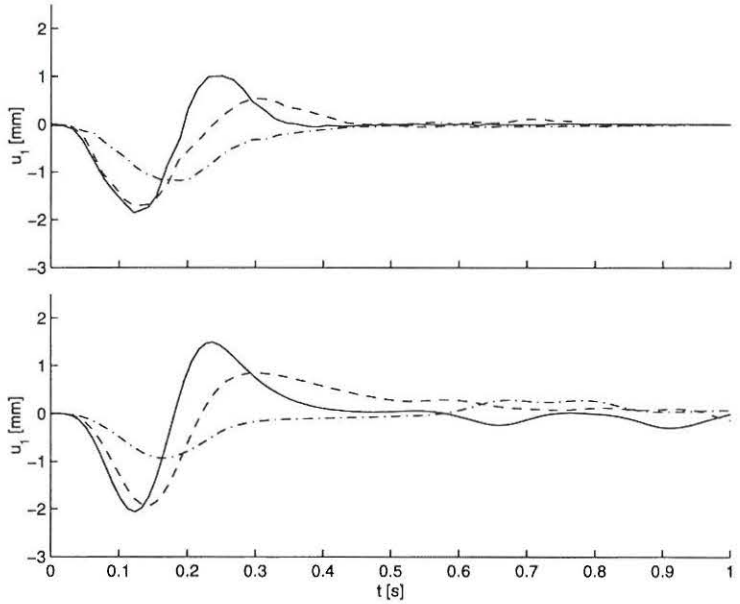

Fig. 7. Horizontal displacements at $(\tilde{x}_1, \tilde{x}_2, \tilde{x}_3)$=(+4 m, 0 m, 0 m) obtained using BEM (top) and FEM (bottom) for $v_1 = 0.5 \cdot c_S$ $-$, $v_1 = 0.7 \cdot c_S$ $--$ and $v_1 = 0.9 \cdot c_S$ $-\cdot-$.

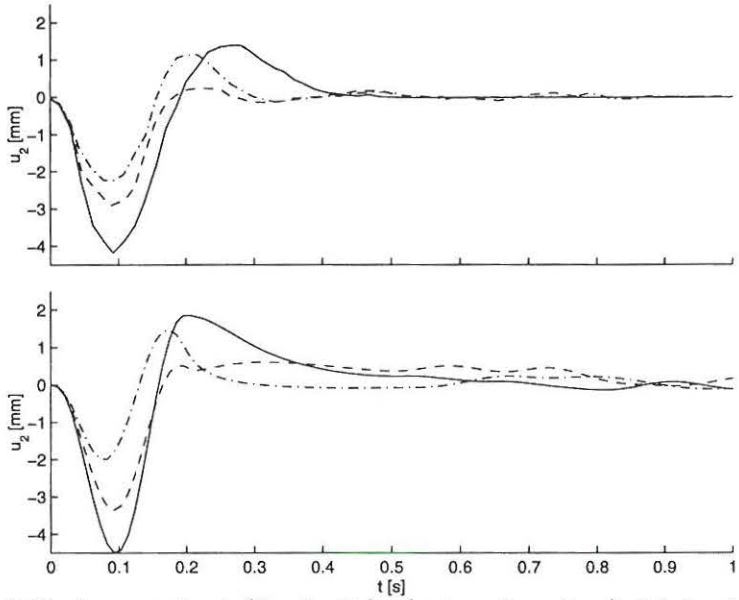

Fig. 8. Vertical displacements at $(\tilde{x}_1, \tilde{x}_2, \tilde{x}_3)$=(+4 m, 0 m, 0 m) obtained using BEM (top) and FEM (bottom) for $v_1 = 0.5 \cdot c_S$ $-$, $v_1 = 0.7 \cdot c_S$ $--$ and $v_1 = 0.9 \cdot c_S$ $-\cdot-$.

The Rayleigh wave velocity for Poisson materials ($\mu = \lambda$) is approximately $0.92 \cdot c_S$. The results for velocities approaching the Rayleigh wave velocity are shown for a point only 4 m in front of force. The reason for this change is that the wavefront in front of the force at the surface do not move very far from the force when the force moves almost as fast as the Rayleigh wave. Krylov [6] assumes that the displacements increases dramatically when the velocity approach the Rayleigh wave velocity. The results in Fig. 7-8 obviously disagrees with that statement. Actually, the displacements decreases compared to the results obtained with lower velocities shown in Fig. 3-6.

7 Conclusion

A new BEM formulation in a moving coordinate system has been given. The formulation introduces Green's functions for a moving force and shows how the normal BEM formulation for a fixed coordinate system can be modified to a formulation in the moving coordinate system by using the Green functions for a moving force.
The BEM results have been compared to results obtained by a FEM formulation using an impedance boundary condition as absorbing boundary.
The results from the BEM and FEM formulation show good agreement for a simple stress wave propagation problem with a moving force and it is demonstrated that the reflection of Rayleigh waves is omitted in the BEM analysis. Another finding is that the displacements do not increase when the velocity approaches the Rayleigh wave velocity as is often postulated.

Acknowledgements

The present research was partially supported by The Danish Technical Research Council within the project: "Damping Mechanisms in Dynamics of Structures and Materials".

References

[1] Banerjee PK, Ahmad S, Manolis GD. Advanced Elastodynamic Analysis, Computational Methods in Mechanics, Volume III. In: Beskos DE. editor. Boundary Element Methods in Mechanics. Elsevier Science Publishers B.V, 1987.

[2] Chouw N, Le R, Schmid G. Reduction of Train-induced Vibrations and Waves. Germany: Ruhr-University Bochum, 1993.

[3] Eringen AC, Suhubi ES. Elastodynamics, Volume II, Linear Theory. Academic Press, 1975.

[4] Krenk S, Kirkegaard P.H, Radiation Conditions for Elastic Waves, Technical University of Denmark. (to be published)

[5] Krenk S, Kellezi L, Nielsen SRK, Kirkegaard PH. Finite Element and Transmitting Boundary Conditions for Moving Loads. Proceedings of the 4th European Conference on Structural Dynamics, Eurodyn'99, Praha. 1999;447-452.

[6] Krylov V. Generation of Ground Vibrations by Superfast Trains. Applied Acoustics. 1995;44:149-164.

[7] Madshus C, Bessason B, Hårvik L. Prediction Model for Low Frequency Vibration from High Speed Railways on Soft Ground. Journal of Sound and Vibration. 1996;193(1):195-203.

[8] Nelson JT. Recent Developments in Ground-borne Noise and Vibration Control. Journal of Sound and Vibration. 1996;193(1):367-376.

[9] Okumura Y , Kuno K. Statistical Analysis of Field Data of Railway Noise and Vibration Collected in an Urban Area. Applied Acoustics. 1991;33:263-280.

[10] Rasmussen KM. Stress Wave Propagation in Soils Modelled by the Boundary Element Method. Pd.D. thesis, Aalborg University, 1999.

[11] Rasmussen KM, Nielsen SRK. 2D Time Domain Boundary Element Direct and Indirect Formulation Applied to Soil Dynamics. Proceedings of the 13th International Conference on Boundary Element Technology, BETECH 99, Las Vegas. 1999;195-204.

[12] Trochides A. Ground-Borne Vibrations in Buildings Near Subways. Applied Acoustics. 1991;32:289-296.